Direct measurement of band offsets on selective area grown In0.53Ga0.47As/InP heterojunction with multiple probe scanning tunneling microscopy

Nemanja Peric, Corentin Durand, Maxime Berthe, Yan Lu, Kekeli N'Konou, B. Grandidier, Roland Coratger, Isabelle Lefebvre, Philipp Ebert, Louis Biadala, et al.

Applied Physics Letters

RESEARCH ARTICLE | NOVEMBER 07 2022

Direct measurement of band offsets on selective area grown $In_{0.53}Ga_{0.47}As/InP$ heterojunction with multiple probe scanning tunneling microscopy

Nemanja Peric; Corentin Durand; Maxime Berthe; ... et. al

Appl. Phys. Lett. 121, 192104 (2022)
https://doi.org/10.1063/5.0104807

Articles You May Be Interested In

Design and properties of planar-type tunnel FETs using $In_{0.53}Ga_{0.47}As/In_xGa_{1-x}As/In_{0.53}Ga_{0.47}As$ quantum well

Journal of Applied Physics (October 2017)

A crystalline oxide passivation on $In_{0.53}Ga_{0.47}As$ (100)

Journal of Applied Physics (March 2017)

Inversion in the $In_{0.53}Ga_{0.47}As$ metal-oxide-semiconductor system: Impact of the $In_{0.53}Ga_{0.47}As$ doping concentration

Appl. Phys. Lett. (January 2017)

Direct measurement of band offsets on selective area grown $In_{0.53}Ga_{0.47}As/InP$ heterojunction with multiple probe scanning tunneling microscopy

Cite as: Appl. Phys. Lett. **121**, 192104 (2022); doi: 10.1063/5.0104807
Submitted: 21 June 2022 · Accepted: 14 October 2022 ·
Published Online: 7 November 2022

View Online Export Citation CrossMark

Nemanja Peric,[1] Corentin Durand,[2] Maxime Berthe,[1] Yan Lu,[3] Kekeli N'Konou,[1] Roland Coratger,[4] Isabelle Lefebvre,[1] Philipp Ebert,[3] Louis Biadala,[1] Ludovic Desplanque,[1] Xavier Wallart,[1] and B. Grandidier[1,a)]

AFFILIATIONS

[1]University Lille, CNRS, Centrale Lille, University Polytechnique Hauts-de-France, Junia-ISEN, UMR 8520 - IEMN, F-59000 Lille, France
[2]LAAS-CNRS, Université de Toulouse, CNRS, UPS, Toulouse F-31400, France
[3]Ernst Ruska-Centrum (ER-C-1) and Peter Grünberg Institut (PGI-5), Forschungszentrum Jülich GmbH, 52425 Jülich, Germany
[4]SINANO Group, CEMES-CNRS and Université Paul Sabatier, Toulouse 31055, France

[a)]Author to whom correspondence should be addressed: bruno.grandidier@univ-lille.fr

ABSTRACT

The knowledge of the band alignment in semiconductor heterostructures is crucial, as it governs carrier confinement with many impacts on the performances of devices. By controlling the direction of the current flow in in-plane $In_{0.53}Ga_{0.47}As/InP$ heterostructure nanowires, either horizontally along the nanowires or vertically into the InP substrate with low temperature multiple-probe tunneling spectroscopy, a direct measurement of the band offsets at the buried $In_{0.53}Ga_{0.47}As/InP$ heterointerface is performed. Despite the unavoidable processing steps involved in selective area epitaxy, conduction and valence band offsets of 0.21 ± 0.01 and 0.40 ± 0.01 eV are, respectively, found, indicating the formation of an interface with a quality comparable to two-dimensional $In_{0.53}Ga_{0.47}As/InP$ heterostructures.

Selective area epitaxy (SAE), which relies on the controlled growth of semiconductor materials into a pattern transferred from a dielectric mask, has been essential to the continuous miniaturization of optoelectronic devices.[1] Photonic integrated circuits have largely benefited from this technique,[2,3] through the monolithic integration of III–V compounds onto silicon substrates.[4,5] Moreover, progresses in the control of the growth within the exposed regions of the substrate and its inhibition on the dielectric mask enable the creation of scalable and complex planar interconnected structures suitable for the transfer of quantum information.[6–10] While the key assets of SAE to produce devices reside in a limited number of processing steps and a significant reduction of threading dislocations in lattice mismatch systems, the lithographic process is bound to bring some contamination before the growth resumes. Stacking faults might also exist when materials with large lattice mismatch are integrated.[11] Both effects can alter the chemistry of heterointerfaces, with a strong impact on the band discontinuities.

To measure the band discontinuities of semiconductor heterostructures, a wide variety of techniques have been developed, including transport measurements, photoemission, and optical spectroscopy.[12] Of particular interest for confined structures is the use of scanning probe microscopy, which enables a direct access to the band alignment with high spatial resolution.[13–16] For III–V heterostructures, scanning tunneling spectroscopy (STS) requires to cleave the material and expose a {110} face, which is naturally passivated.[17,18] However, in recent years, it has been shown that STS can also resolve the band offset for buried heterointerfaces.[19,20] Such an approach is valid, when the conduction (CB) or valence (VB) band edges of the material exposed to the probe are higher or lower than the edges of the material underneath, so that the top material is electronically transparent to the tunneling electrons within a limited energy window. For SAE nanowire (NW) networks engineered for quantum computing, the nanowires (NWs) usually consist of narrow bandgap materials.[8–10,21,22] Hence, it makes this condition obsolete and calls for the design of experimental schemes suitable for the band offset measurement of buried heterointerfaces.

Here, as a prototypical example, we investigate the band discontinuities of $In_{0.53}Ga_{0.47}As$ NWs grown by SAE on an InP (001) substrate. This heterostructure with a type I band alignment was thoroughly characterized for quantum wells[23–26] and is of current interest in III–V transistor technologies integrated on Si.[27] Moreover, $In_{0.53}Ga_{0.47}As$ NWs have recently been grown on InP using SAE.[28–30] By implementing a technique based on multiple-tip STS to study the heterojunction parameters, we show that the CB and VB offsets of the buried $In_{0.53}Ga_{0.47}As$/InP interface can be accurately determined. The measured band offsets are consistent with the ones encountered for two-dimensional lattice-matched $In_{0.53}Ga_{0.47}As$/InP heterostructures. Such a result indicates that the procedure to remove the oxide and produce a clean and ordered InP surface in the mask opening, without the need of an intermediate buffer layer, is effective and gives rise to the formation of high quality interfaces.

As SAE involves a growth inside apertures defined in a dielectric mask, a 30 nm-thick SiO_2 layer was deposited by plasma enhanced chemical vapor deposition on *p*-type InP (001) substrates with a Zn concentration of 3×10^{18} cm^{-3}. The samples were further covered with a resist, which was modified with e-beam lithography to design apertures of different sizes and geometry. To transfer these patterns, the SiO_2 layer was etched in two steps: first, by means of reactive ion etching, and, following the resist removal, by a smooth chemical etching with diluted hydrofluoric acid. The thickness of the remaining SiO_2 mask outside the apertures was about 10 nm. Then, the wafer was loaded into the growth reactor and annealed under ultra-high vacuum (UHV) at 200 °C for one hour. The InP surface inside the mask apertures was deoxidized and cleaned using atomic hydrogen under As_4 flux. Lattice-matched $In_{0.53}Ga_{0.47}As$ NWs to InP, with a nominal thickness of 20 nm, were grown with molecular beam epitaxy at a growth rate of 0.2 ML s^{-1}, a temperature of 480 °C, and a V/III flux ratio of 2.5.[28] Finally, the NWs were capped with a thin amorphous As layer to protect them from reaction with air during their transfer.

Prior to the analysis of the NWs with UHV scanning electron microscopy (SEM) and scanning tunneling microscopy (STM) (Nanoprobe, Scienta Omicron), the As capping layer was removed by annealing the samples at 320 °C, monitoring the As desorption with mass spectroscopy. For all STM experiments, the SEM was used to locate the NWs and guide the coarse approach of the STM tips toward the NWs, avoiding any harmful landing on the SiO_2 surface. Once the NWs had been characterized in UHV at a temperature of 5 K, they were further observed with tapping mode atomic force microscopy (AFM) under standard atmospheric conditions (D3100, Bruker). In order to precisely determine the geometry of the facets, cross sections were prepared by milling thin slices, perpendicular to the NW main axis, with the use of a focused ion beam machine. The slices were analyzed with scanning transmission electron microscopy (STEM) using a Cs-probe corrected FEI Titan 80–200 microscope and an accelerating voltage of 200 kV.

For this study, we considered single $[1\bar{1}0]$-oriented NWs or $[1\bar{1}0]$-oriented NWs belonging to crossbar structures, all having a width of 500 nm and a length of 10 μm. As shown from the analysis of the morphology in Fig. 1, the NWs have a trapezoidal shape with a (001) top facet and two tilted side facets. As both facets make an angle of $\sim$19.5° with the plane-parallel to the substrate, they correspond to {114} side facets. Based on the homogeneous AFM contrast of the $[1\bar{1}0]$-oriented NW seen in Fig. 1(b), the top facet is rather flat, which is confirmed by the atomically resolved STM image of Fig. 1(c). It consists of terraces and islands, separated by single atomic step height. Their surface shows $[1\bar{1}0]$-elongated rows of small bright protrusions. This structure is consistent with an As-rich (2 × 4) reconstruction,[31] which is expected for an InGaAs (001) surface after the sublimation of the amorphous As protecting layer.[32,33] Moreover, the study of the

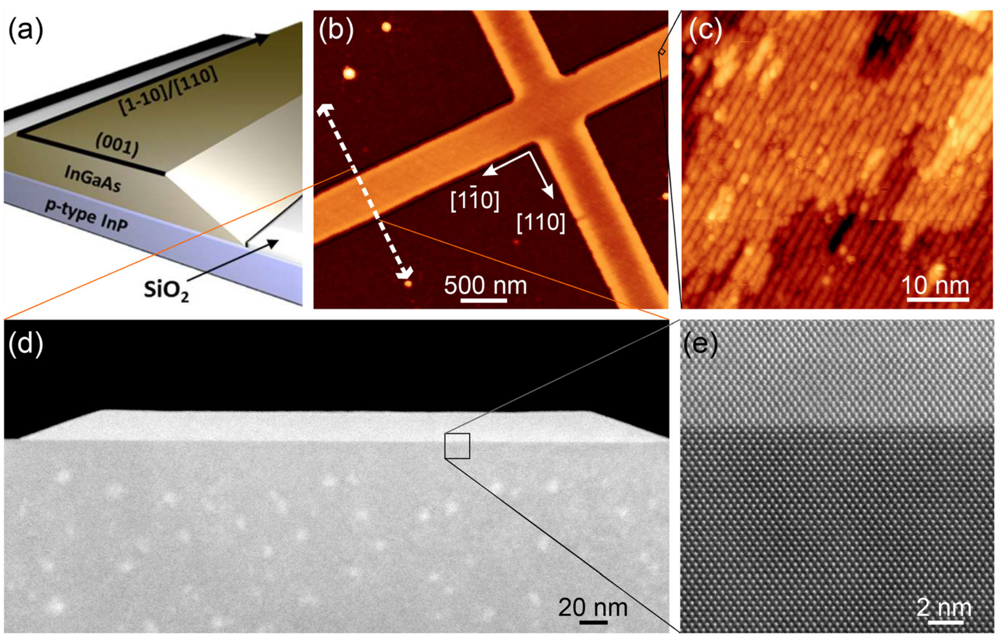

FIG. 1. (a) Schematic of the InGaAs NWs grown by selective area epitaxy on an InP(001) surface. (b) AFM image of two NWs arranged in a crossbar structure. (c) High resolution STM image of the InGaAs (001)-(2 × 4) reconstruction observed on the top facet of the NW grown along the $[1\bar{1}0]$ direction. (d) Cross-sectional STEM image of the InGaAs/InP heterostructure acquired across the InGaAs NW as defined by the dashed segment in (b). (e) High resolution STEM image of the InGaAs/InP heterointerface.

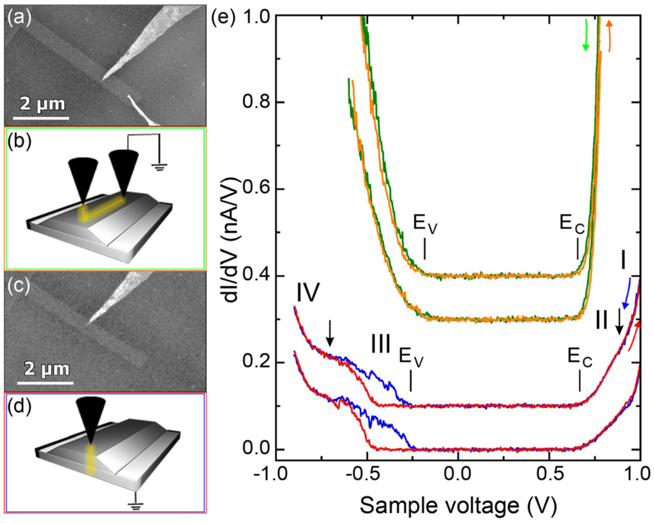

FIG. 2. (a) and (c) SEM images and (b) and (d) schematics of the current paths for two-tip and single-tip spectroscopy. (e) dI/dV spectra acquired with two-tip (upper curves) and single-tip (lower curves) spectroscopy at two different locations on the top (001) facet of an $In_{0.53}Ga_{0.47}As$ NW at 5 K. The different transport regimes I, II, III, and IV, described in Fig. 3, are separated by the conduction E_C and valence E_V band edges and vertical arrows. The tilted downward and upward curved arrows indicate the forward and backward voltage sweeps, respectively. Feedback parameters for the upper curves, $V_s = +0.8$ V, $I_t = 60$ pA, and for the lower curves, $V_s = +1.0$ V, $I_t = 30$ pA.

InGaAs/InP interface by cross-sectional STEM reveals an atomically sharp interface with well-matched atomic columns between the InP substrate and the InGaAs NW [Fig. 1(e)], in agreement with the intended growth of lattice matched $In_{0.53}Ga_{0.47}As$ NWs.

The high quality of the interface and the clean and well-ordered (001) top facet of the $In_{0.53}Ga0_{.47}As$ NWs serve as a good test bed for the investigation of the $In_{0.53}Ga_{0.47}As$/InP heterointerface with multiple-probe tunneling spectroscopy (see the supplementary material for the experimental details). As shown in Fig. 2, two different configurations in the position of the electrical ground contact were studied. For the first one [Fig. 2(a)], the electrical ground contact is provided by a tungsten tip pressed onto the top facet of the NW (the substrate is disconnected from the ground). This ground contact was established by first approaching one of the two tungsten tips of the multiple-probe STM using the distance regulation of the STM control system, followed by a push down of the tip onto the NW top facet in the feedback-off mode. At contact, the monitored current exhibits a significant jump. The second tip on the NW is kept in the constant-current STM mode and is separated from the tip in contact with the top facet of the NW by a distance varying between 0.9 μm and 1.5 μm. Aplying the voltage to the tunneling tip and the ground to the tip in contact, a current flows parallel to the $[1\bar{1}0]$ direction. It is mostly confined in the NW [Fig. 2(b)], due to the potential barrier existing at the heterointerface (see Fig. 3). Sweeping the bias forward and backward yields reproducible dI/dV spectra [upper curves in Fig. 2(e)]. The positive and negative branches correspond to tunneling into and out of the CB and VB, respectively. They are separated by a zero conductance

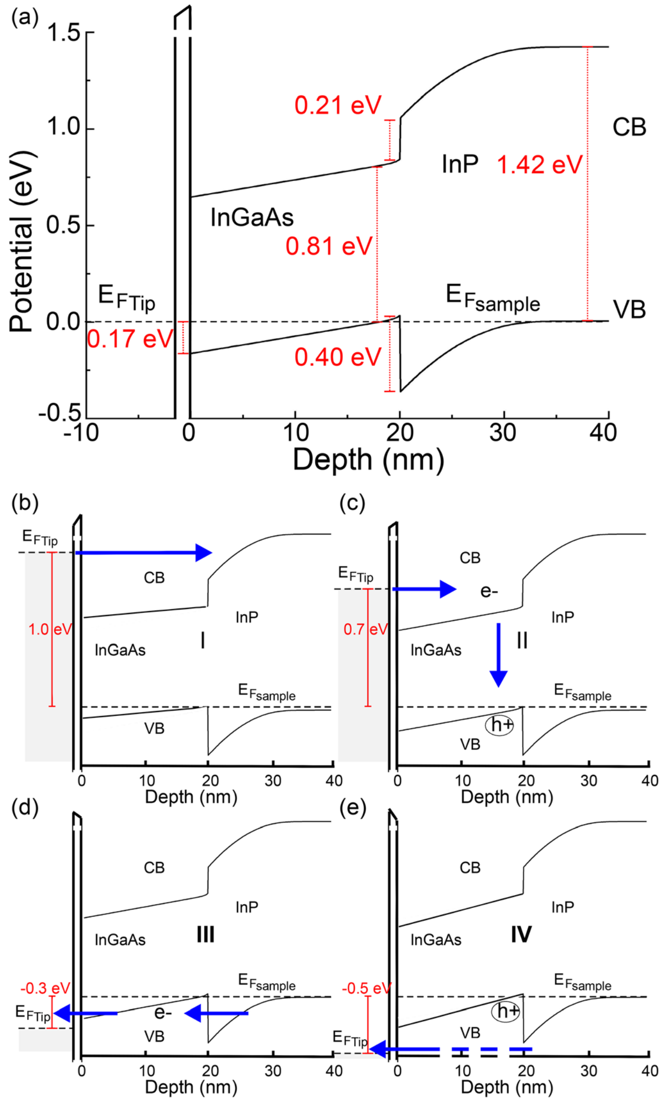

FIG. 3. (a) COMSOL-simulated band diagram of the metal-vacuum-$In_{0.53}Ga_{0.47}As$/InP junction at 5 K for zero bias. The values of the Fermi level pinning at the surface of the NW, the band gaps of the InGaAs NW and the InP substrates, and the conduction and valence band offsets deduced from the measurements are indicated. (b)–(e) Band diagrams corresponding to the different transport regimes found in single-tip tunneling spectroscopy. The conduction and valence bands are labeled CB and VB, respectively. The arrows highlight the transfer of charge carriers. The nature of the charge carriers is indicated, when the transfer involves a two-step process or a charging effect.

region (ZCR) of 0.81 ± 0.01 V, defined as the region where the tunneling current reaches the experimental noise level.

Although not visible as peaks in the dI/dV characteristics, the existence of the surface states related to the As-rich (2×4) reconstruction of the (001) facet is disclosed by the position of the Fermi level at zero volt relative to the band edges. More precisely, the measured energy position of the Fermi level of 0.17 ± 0.01 eV above the VB edge points to a pinning of the Fermi level by intrinsic defects behaving as surface donors.[34] The related surface states are known to provide a significant conductivity when measured with four-probe STM.[33] Moreover, this surface pinning along with the high doping of the InP substrate causes the formation of an accumulation of holes in the InGaAs layer toward the heterointerface, which is also conductive [Fig. 3(a)]. As a result, the electrical resistance between the point of the surface facing the tunneling tip apex and the tip in contact with the top facet is much smaller than the tunneling resistance. As the potential mostly drops across the tunneling junction, the ZCR measured by STS corresponds to the bandgap of the NW.[35] The experimental value agrees well with the bulk bandgap of $In_{0.53}Ga_{0.47}As$ at low temperature, 0.816 eV.[36]

In the second configuration [Fig. 2(c)], only one tunneling tip is used, and the substrate is connected to the ground. The current of tunneling electrons flows now from the tunneling tip across the $In_{0.53}Ga_{0.47}As$/InP heterointerface to the backside electrical ground contact [Fig. 2(d)]. Again, the dI/dV spectra show two branches corresponding to tunneling into and out of CB and VB at positive and negative bias, respectively [lower curves in Fig. 2(e)]. However, marked differences exist as compared to the spectra measured using the two-tip configurations. The ZCR is slightly wider when the forward bias sweep, starting at positive bias, is considered (0.92 ± 0.01 eV). Also, the dI/dV signal is noisy at the top of the VB and exhibits a hysteresis, making the ZCR much larger in the backward bias sweep. Then, onsets, corresponding to a sudden increase in the tunneling current, are observed in the CB and VB as marked by the downward pointing arrows at bias of 0.92 V and -0.71 V, respectively. The onset measured at positive bias is specific to the single-tip configuration, as the dI/dV and $I(V)$ characteristics measured with two tips monotonically increase in the same voltage range (see the supplementary material, Fig. S3).

In contrast to the two-probe tunneling spectroscopy, the electrical contact is located at the back of the InP substrate. As the Fermi level is pinned at the top facet of the $In_{0.53}Ga_{0.47}As$ NW, the high doping of the InP substrate imposes a downward bending of the bands across the heterointerface to satisfy the condition of electroneutrality at zero volt [Fig. 3(a)]. The depletion of free holes in the InP side of the heterojunction leads to the formation a space charge region, which can be modeled by a tunneling junction. Hence, the $In_{0.53}Ga_{0.47}As$ NW is coupled to the STM tip and the p-type doped InP substrate via two tunnel junctions. In this geometry, the applied voltage is distributed across both tunneling junctions, and the width of the zero-conductance region is related to the bandgap by the lever arm, which corresponds to the ratio between the potential drop across the NW-tip junction and the applied voltage. Based on the width of the ZCR and the measured bandgap from the two-tip configuration, a lever arm of 0.88 is obtained.

At high positive bias, tunneling electrons from the tip are transferred to the Bloch states of the InGaAs NW, which are coupled to the InP substrate. The electrons can, therefore, reach the CB of the InP substrate [Fig. 3(b)]. When the bias is reduced and the tip's Fermi level becomes lower than the onset of the band discontinuity between the InGaAs and InP layers, the electrons cannot escape to the CB of InP any more [Fig. 3(c)]. At a temperature of 5 K, the only exit path is to recombine with the free holes in the VB of the InGaAs NW.[33] This transition in the current flow translates into a change in the slope of the dI/dV signal, as observed at $+0.92$ V [highlighted by a vertical arrow in Fig. 2(e)]. Therefore, the difference of bias measured between the inflection point and the bottom of the CB gives access to the CB offset. Due to the partial drop of the applied bias in the InP space charge region, the CB offset is obtained by multiplying this difference with the lever arm, yielding 0.21 ± 0.01 eV. Such a value is consistent with the band offsets measured in two-dimensional $In_{0.53}Ga_{0.47}As$/InP heterostructures with other techniques,[23–25] although some small deviations might exist depending on the quality of the heterointerface.[26]

At negative bias, electrons tunnel out from the VB states of the NW into empty tip states. The electrons leave behind empty states (holes). For the energy window defined by the VB offset of the heterojunction, the probability to refill these states with electrons tunneling from the InP VB through the space charge might be smaller than the probability to tunnel across the NW-tip junction [Fig. 3(d)]. As a result, the NW gets charged with holes, accounting for the appearance of noise and the clear hysteresis observed between the forward and backward voltage sweeps.[37,38] When the bias decreases further, the VB states of the NW become coupled with those of the InP substrate, and electrons do not have to tunnel across the space charge layer, making the transport more efficient [Fig. 3(e)]. Hence, the difference of bias between the top of the VB and the inflection point measured at negative bias provides the height of the band discontinuity in the VB. Converting this difference into energy yields a VB offset of 0.40 ± 0.01 eV, in agreement with the literature.[25] Adding both, the CB and VB offsets to the measured bandgap of the NW (0.81 eV) give an energy of 1.42 eV, which corresponds to the bandgap of InP at low temperature.[20]

While the measurement of the apparent bandgap with the single-tip configuration is found to be the same at different positions of the NW within the precision of ± 0.01 eV, variations slightly larger than the experimental precision exist for the onsets related to the band offsets. As observed in Figs. 2 and S2 (see the supplementary material), fluctuations of the conduction and valence band offsets, not larger than 0.23 and 0.44 eV, respectively, can be found here and there, calling for future works involving additional experimental techniques to correlate these shifts with the structural properties of the buried interface.

In summary, $In_{0.53}Ga_{0.47}As$ NWs were grown by SAE on a p-type InP (001) substrate. Although the heterointerface is located around 20 nm below the top facet of the NW, our experimental scheme provides a direct access to the band offsets. The method relies on the experimental knowledge of the potential distribution, which is essential to convert the measured voltage separations into the band offsets, a property that cannot be obtained with single-probe tunneling spectroscopy only. It is suitable for NW, but it could be applied to two-dimensional heterostructures as well. As in both configurations, only one tip is tunneling, the scanning ability of the tunneling tip opens the door to map electronic inhomogeneities at the heterointerfaces with a high spatial resolution.

See the supplementary material for the experimental details about the STS experiments, the determination of the band offsets, and additional spectra measured with the single or two-tip configuration.

This study was financially supported by the European Community's H2020 Program (Grant No. PITN-GA-2016-722176, "Indeed" Project), the EQUIPEX program Excelsior (Grant No.

ANR-11-EQPX-0015), the IEMN CMNF and PCMP-PCP platforms of the RENATECH network, and the Deutsche Forschungsgemeinschaft (Grant No. 390247238).

AUTHOR DECLARATIONS

Conflict of Interest

The authors have no conflicts to disclose.

Author Contributions

Nemanja Peric: Conceptualization (equal); Data curation (lead); Formal analysis (lead); Funding acquisition (equal); Project administration (equal); Supervision (equal); Writing – original draft (equal). **Ludovic Desplanque:** Investigation (equal); Methodology (equal); Supervision (equal); Writing – review & editing (equal). **Xavier Wallart:** Investigation (equal); Writing – review & editing (equal). **Bruno Grandidier:** Conceptualization (equal); Funding acquisition (equal); Investigation (equal); Project administration (equal); Supervision (equal); Writing – original draft (equal); Writing – review & editing (equal). **Corentin Durand:** Data curation (equal); Formal analysis (lead); Investigation (equal). **Maxime Berthe:** Formal analysis (equal); Investigation (equal). **Yan Lu:** Investigation (equal); Methodology (equal). **Kekeli N'Konou:** Investigation (equal). **Roland Coratger:** Investigation (equal). **Isabelle Lefebvre:** Investigation (supporting); Software (supporting). **Philipp Ebert:** Investigation (equal); Writing – review & editing (equal). **Louis Biadala:** Methodology (equal); Supervision (equal); Writing – review & editing (equal).

DATA AVAILABILITY

The data that support the findings of this study are available from the corresponding author upon request.

REFERENCES

[1] P. D. Dapkus, C. Y. Chi, S. J. Choi *et al.*, Prog. Quantum Electron. **75**, 100304 (2021).
[2] Y. D. Galeuchet, P. Roentgen, and V. Graf, J. Appl. Phys. **68**, 560 (1990).
[3] J. J. Coleman, R. M. Lammert, M. L. Osowski, and A. M. Jones, IEEE J. Sel. Top. Quantum Electron. **3**, 874 (1997).
[4] Y. Ujiie and T. Nishinaga, Jpn. J. Appl. Phys., Part 2 **28**, L337 (1989).
[5] H. Schmid, M. Borg, K. Moselund, L. Gignac, C. M. Breslin, J. Bruley, D. Cutaia, and H. Riel, Appl. Phys. Lett. **106**, 233101 (2015).
[6] J. Gooth, M. Borg, H. Schmid, V. Schaller, S. Wirths, K. Moselund, M. Luisier, S. Karg, and H. Riel, Nano Lett. **17**, 2596 (2017).
[7] M. Friedl, K. Cerveny, P. Weigele, G. Tütüncüoglu, S. Martí-Sánchez, C. Huang, T. Patlatiuk, H. Potts, Z. Sun, M. O. Hill, L. Güniat, W. Kim, M. Zamani, V. G. Dubrovskii, J. Arbiol, L. J. Lauhon, D. M. Zumbühl, and A. Fontcuberta i Morral, Nano Lett. **18**, 2666 (2018).
[8] S. Vaitiekėnas, A. M. Whiticar, M.-T. Deng, F. Krizek, J. E. Sestoft, C. J. Palmstrøm, S. Martí-Sánchez, J. Arbiol, P. Krogstrup, L. Casparis, and C. M. Marcus, Phys. Rev. Lett. **121**, 147701 (2018).
[9] P. Aseev, A. Fursina, F. Boekhout, F. Krizek, J. E. Sestoft, F. Borsoi, S. Heedt, G. Wang, L. Binci, S. Martí-Sánchez, T. Swoboda, R. Koops, E. Uccelli, J. Arbiol, P. Krogstrup, L. P. Kouwenhoven, and P. Caroff, Nano Lett. **19**, 218 (2019).
[10] R. L. M. Op het Veld, D. Xu, V. Schaller, M. A. Verheijen, S. M. E. Peters, J. Jung, C. Tong, Q. Wang, M. W. A. de Moor, B. Hesselmann, K. Vermeulen, J. D. S. Bommer, J. S. Lee, A. Sarikov, M. Pendharkar, A. Marzegalli, S. Koelling, L. P. Kouwenhoven, L. Miglio, C. J. Palmstrøm, H. Zhang, and E. P. A. M. Bakkers, Commun. Phys. **3**, 59 (2020).
[11] M. Fahed, L. Desplanque, D. Troadec, G. Patriarche, and X. Wallart, J. Cryst. Growth **477**, 45 (2017).
[12] A. Franciosi and C. G. Van de Walle, Surf. Sci. Rep. **25**, 1–140 (1996).
[13] D. Steiner, D. Dorfs, U. Banin, F. Della Sala, L. Manna, and O. Millo, Nano Lett. **8**, 2954 (2008).
[14] W. Melitz, J. Shen, A. C. Kummel, and S. Lee, Surf. Sci. Rep. **66**(1), 1–27 (2011).
[15] C. Zhang, M. Y. Li, J. Tersoff, Y. Han, Y. Su, L. J. Li, D. A. Muller, and C. K. Shih, Nat. Nanotechnol. **13**, 152 (2018).
[16] W. Peng, H. Wang, H. Lu, L. Yin, Y. Wang, B. Grandidier, D. Yang, and X. Pi, Small **17**, 2100655 (2021).
[17] O. Albrektsen, D. J. Arent, H. P. Meier, and H. W. M. Salemink, Appl. Phys. Lett. **57**, 31 (1990).
[18] Y. Dong, R. M. Feenstra, M. P. Semtsiv, and W. T. Masselink, J. Appl. Phys. **103**, 073704 (2008).
[19] T. Xu, M. J. Wei, P. Capiod, A. Díaz Álvarez, X. L. Han, D. Troadec, J. P. Nys, M. Berthe, I. Lefebvre, G. Patriarche, S. R. Plissard, P. Caroff, Ph. Ebert, and B. Grandidier, Appl. Phys. Lett. **107**, 112102 (2015).
[20] L. Biadala, W. Peng, Y. Lambert, J. H. Kim, D. Canneson, A. Houppe, M. Berthe, D. Troadec, D. Deresmes, G. Patriarche, T. Xu, X. Pi, X. Wallart, C. Delerue, M. Bayer, J. Xu, and B. Grandidier, ACS Nano **13**, 1961 (2019).
[21] J. Jung, R. L. Op het Veld, R. Benoist, O. A. van der Molen, C. Manders, M. A. Verheijen, and E. P. A. M. Bakkers, Adv. Funct. Mater. **31**, 2103062 (2021).
[22] M. Fahed, L. Desplanque, D. Troadec, G. Patriarche, and X. Wallart, Nanotechnology **27**, 505301 (2016).
[23] M. A. Haase, N. Pan, and G. E. Stillman, Appl. Phys. Lett. **54**, 1457 (1989).
[24] A. W. Higgs, H. J. Hutchinson, L. L. Taylor, N. Apsley, and S. J. Bass, Semicond. Sci. Technol. **5**, 581 (1990).
[25] J. R. Waldrop, E. A. Kraut, C. W. Farley, and R. W. Grant, J Appl. Phys. **69**, 372 (1991).
[26] P. E. Smith, S. H. Goss, M. Gao, M. K. Hudait, Y. Lin, S. A. Ringel, and L. Brillson, J. Vac. Sci. Technol., B **23**, 1832 (2005).
[27] D. Caimi, H. Schmid, T. Morf, P. Mueller, M. Sousa, K. E. Moselund, and C. B. Zota, Solid State Electron. **185**, 108077 (2021).
[28] A. Bucamp, C. Coinon, J. L. Codron, D. Troadec, X. Wallart, and L. Desplanque, J. Cryst. Growth **512**, 11–15 (2019).
[29] Y. P. Liu, L. Södergren, S. F. Mousavi, Y. Liu, F. Lindelöw, E. Lind, R. Timm, and A. Mikkelsen, Appl. Phys. Lett. **117**, 163101 (2020).
[30] M. E. Cachaza, A. W. Christensen, D. Beznasyuk, T. Særkjær, M. H. Madsen, R. Tanta, G. Nagda, S. Schuwalow, and P. Krogstrup, Phys. Rev. Mater. **5**, 094601 (2021).
[31] M. D. Pashley, K. W. Haberern, W. Friday, J. M. Woodall, and P. D. Kirchner, Phys. Rev. Lett. **60**, 2176 (1988).
[32] J. Shen, D. L. Winn, W. Melitz, J. B. Clemens, and A. C. Kummel, ECS Trans. **16**, 463 (2008).
[33] N. F. Vergel, A. Tadjine, V. Notot, M. Mohr, A. K. N'guissan, C. Coinon, M. M. Dzagli, J.-C. Girard, G. Rodary, L. Desplanque, R. Berndt, D. Stiévenard, X. Wallart, C. Delerue, and B. Grandidier, Phys. Rev. Mater. **3**, 094604 (2019).
[34] M. D. Pashley, K. W. Haberern, R. M. Feenstra, and P. D. Kirchner, Phys. Rev. B **48**, 4612 (1993).
[35] F. Flores and N. Garcia, Phys. Rev. B **30**, 2289 (1984).
[36] I. Vurgaftman, J. R. Meyer, and L. R. Ram-Mohan, J. Appl. Phys. **89**, 5815 (2001).
[37] M. R. Hummon, A. J. Stollenwerk, V. Narayanamurti, P. O. Anikeeva, M. J. Panzer, V. Wood, and V. Bulović, Phys. Rev. B **81**, 115439 (2010).
[38] N. Peric, Y. Lambert, S. Singh, A. Hossain Khan, N. A. Franchina Vergel, D. Deresmes, M. Berthe, Z. Hens, I. Moreels, C. Delerue, B. Grandidier, and L. Biadala, Nano Lett. **21**, 1702 (2021).